Journal of Low Temperature Physics, Vol. 129, Nos. 1/2, October 2002 (© 2002)

Thermodynamic Properties of Superfluid ^{4}He at Negative Pressure

H. J. Maris[1] and D. O. Edwards[2]

[1] *Department of Physics, Brown University, Providence, Rhode Island 02912*
E-mail: humphrey_maris@brown.edu
[2] *Department of Physics, The Ohio State University, Columbus, Ohio 43210*
E-mail: edwards@mps.ohio-state.edu

(Received May 17, 2002; revised June 7, 2002)

We calculate the thermodynamics of superfluid ^{4}He at negative pressures. We use the Landau theory in which thermodynamic properties are expressed as sums over the thermal distribution of elementary excitations. The excitation dispersion curve is taken from the density functional theory developed by Dalfovo et al. *To give a good description of the liquid near to the lambda line, we include the interaction between the elementary excitations using a modification of the roton liquid theory of Bedell, Pines, and Fomin. The calculated quantities include the location of the lambda line, the liquid-vapor spinodal, and lines of constant entropy in the pressure-temperature* (P-T) *plane. We have also calculated the line of minimum density (zero expansion coefficient) in the* P-T *plane. This joins the lambda line tangentially at about −5.3 bars. Using the critical properties near the lambda line, we find that the line of maximum density in He I also joins the lambda line tangentially at this pressure. For use in cavitation experiments, we have calculated the states on the lambda line reached by isentropic expansion from He I.*

1. INTRODUCTION

During the last few years a number of experiments[1,2] have been performed to learn about the behavior of liquid helium at pressures that are negative[3] with respect to the liquid-vapor phase equilibrium pressure. Most of this work has been directed toward the investigation of the nucleation of vapor bubbles in the liquid. Since helium remains liquid down to absolute zero, it is possible to study this nucleation process down to very low temperatures and to investigate the nucleation of bubbles that takes place via quantum tunneling.[4,5] Recently, preliminary work has begun on an experimental determination of the equation of state of helium at negative pressures.[6]

0022-2291/02/1000-0001/0 © 2002 Plenum Publishing Corporation

In the analysis of these experiments, it would be very helpful to have some estimate of the thermodynamic properties of helium at negative pressures. In particular, since negative pressures are achieved by rapid adiabatic expansion, one would like to know the properties of the liquid along lines of constant entropy. For any substance, one way to estimate properties at negative pressure is to perform some type of extrapolation of measurements that have been made in the positive pressure regime. Such an extrapolation of the thermodynamic functions has already been made for liquid ^{4}He in the normal phase above the lambda temperature T_λ.[7] For the superfluid phase, there is another way to extrapolate the thermodynamic functions. Landau[8] derived expressions for the thermodynamic functions of superfluid helium in terms of the dispersion curve for elementary excitations (phonons and rotons) in the liquid. In this paper, we present calculations of the thermodynamic properties of superfluid ^{4}He at negative pressures using the Landau approach. Wherever possible, we compare our results with those obtained by Monte Carlo calculations[9] or the direct use of density functional theory. Using the Landau approach and the known critical behavior near the lambda line, we have been able to answer some of the questions raised by Skripov[10] about the line of minimum density (zero expansion coefficient) at negative pressures.

2. THE EQUATION OF STATE AT NEGATIVE PRESSURES

According to the Landau theory, the energy of superfluid helium at finite temperature is the energy at the same density at $T = 0$ plus the energy of the thermally excited elementary excitations. Thus, the internal energy $e(\rho, T)$ per unit volume when the density is ρ is

$$e(\rho, T) = e(\rho, 0) + \frac{1}{V} \sum_{\vec{q}} n_{\vec{q}} \varepsilon_{\vec{q}} + \cdots, \tag{1}$$

where $n_{\vec{q}}$ is the Bose distribution function, and $\varepsilon_{\vec{q}}$ is the energy of an excitation of wave vector $\vec{q}$ at $T = 0$. The sum over states is for volume V. Thus to construct the thermodynamic functions, it is necessary to have an estimate of both $e(\rho, 0)$, obtained from the equation of state at $T = 0$ K, and the dispersion relation. $\varepsilon_{\vec{q}}$ as a function of density. In addition, particularly near the λ-line, Eq. (1) is not adequate without the third term indicated by the dots. The third term describes the effect of the interactions between the excitations. This is discussed in Sec. IV. When the interactions are included, Eq. (1) is replaced by Eq. (7) below.

(a) Energy at Zero Temperature

There have been a number of estimates and calculations of the ground state energy of helium at negative pressures, and we review these briefly here. One approach is based on the very accurate measurements made by Abraham *et al.*[11] of the sound velocity c at positive pressures and at temperatures below 0.1 K. The temperature-dependence of c below 0.1 K is of the order of 1 ppm,[12] so that the results are effectively for $T = 0$. Xiong and Maris[13] fit these data for $c(P)$ to a Padé approximant, and then used the approximant to extrapolate the sound velocity into the negative pressure regime. It was found that at a critical negative pressure P_c, the sound velocity goes to zero. Different fitting procedures gave different estimates of the pressure at this spinodal, with P_c lying between -8 and -9 bars. In a later analysis,[14] it was noticed that the sound velocity at positive pressures could be fit very well by the law

$$c^3 = b(P - P_c), \tag{2}$$

with b a constant. Assuming that this law continues to hold for negative pressures, the equation of state for negative pressures can be obtained with the results summarized in Appendix A. The sound velocity at $T = 0$ as a function of pressure is shown in Fig. 1, the pressure as a function of density

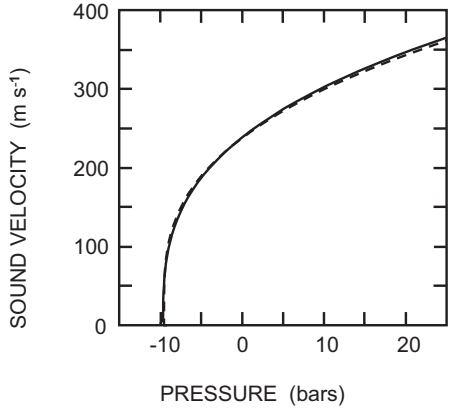

Fig. 1. The sound velocity in ^{4}He at $T = 0$ as a function of pressure. The solid curve is from Eq. (2). The experimental data of Abraham *et al.* (Ref. 11) have a mean deviation from this curve of less than 0.2% which would not be discernible on the scale of the figure. The dashed curve is from the model of Dalfovo *et al.* (Ref. 15).

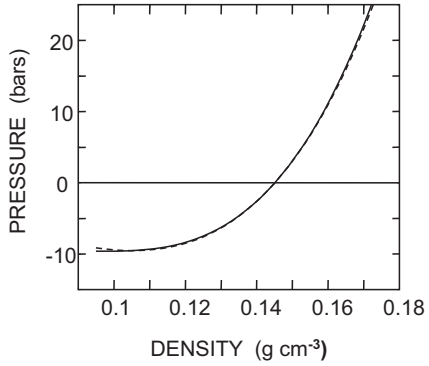

Fig. 2. The pressure in ^{4}He at $T = 0$ as a function of density. The solid line is from Eq. (2), fitted to experimental data at non-negative pressures from Refs. 32 and 11; the dashed line is from the model of Dalfovo *et al.* (Ref. 15). The critical densities in the two calculations are 0.09426 g cm^{-3} for Eq. (2) and 0.01053 g cm^{-3} for Ref. 15. The deviations between the solid curve and the experimental data would be imperceptible on the scale of the graph.

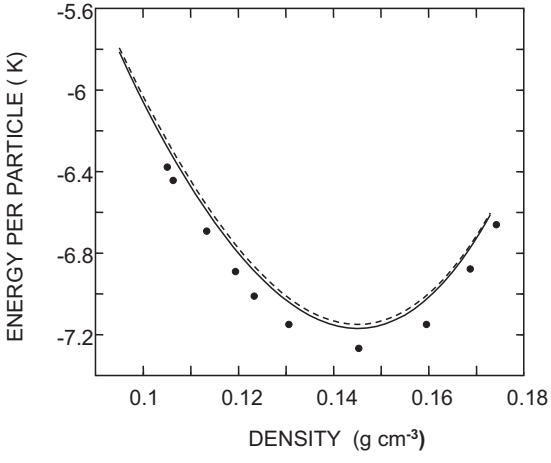

Fig. 3. The energy per particle in K as a function of density at $T = 0$ K in ^{4}He. The solid curve is calculated from Eq. (2), fitted to experimental data at non-negative pressures from Refs. 32 and 11; the dashed line is from the model of Dalfovo *et al.* (Ref. 15). The solid circles are the results of diffusion Monte Carlo calculations by Boronat *et al.*, Ref. 18).

in Fig. 2, and the energy per atom as a function of density in Fig. 3. The sound velocity measurements of Abraham *et al.* are not included in Fig. 1 since the average deviation of the measurements from the fit is extremely small, only 0.43 m s^{-1}.

A second equation of state has been developed by Dalfovo *et al.*[15] They take the energy per particle to be a polynomial in ρ of the form $A_1\rho + A_2\rho^2 + A_3\rho^3$. The coefficients A_i are chosen so as to reproduce the values of the density, energy per particle and compressibility of bulk helium at zero pressure. These are slightly different from those that we would now regard as the best available experimental values.[16] In their model, the energy per unit volume is

$$e(\rho) = a_2\rho^2 + a_3\rho^3 + a_4\rho^4, \tag{3}$$

where with ρ in units of g cm^{-3}, they give the coefficients a_2, a_3 and a_4 as -1.1235×10^9, -5.6703×10^9 and 4.3825×10^{10} cgs units, respectively. Quantities calculated using this equation of state are included in Figs. 1 to 3. According to this model, the spinodal pressure at zero temperature is -9.534 bars compared to -9.620 bars from the fit to Eq. (2) in Appendix A.[17]

Also included in Fig. 3 are the results of quantum Monte Carlo simulations by Boronat *et al.*[18] These give a slightly larger binding energy per particle.

3. DISPERSION CURVE FOR ELEMENTARY EXCITATIONS

The dispersion curve of excitations in superfluid ^{4}He at positive pressures has been studied extensively by neutron scattering,[19] but no data at negative pressures are available.[20,9] Hence, we will use the density functional theory of Dalfovo *et al.*[15] to calculate the excitation energy ε_q as a function of wave number q. For positive pressures, this theory gives results in quite good agreement with experimental measurements. According to Dalfovo *et al.*, the energy ε_q^0 of an excitation at zero temperature is given by

$$(\varepsilon_q^0)^2 = \frac{\hbar^2q^2\{1 - n_4[\hat{V}_J(0) - \hat{V}_J(q)]\}}{m\,|\chi(q)|}, \tag{4}$$

where n_4 is the number density, m is the mass of a ^{4}He atom, $\chi(q)$ is the static response function, and $\hat{V}_J(q)$ is the Fourier transform of the current-current interaction $V_J(r)$ given by

$$V_J(r) = (\gamma_{11} + \gamma_{12}r^2)\exp(-\alpha_1 r^2) + (\gamma_{21} + \gamma_{22}r^2)\exp(-\alpha_2 r^2), \tag{5}$$

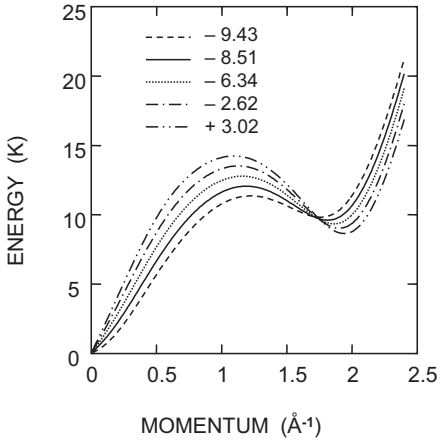

Fig. 4. Dispersion curves for phonons and rotons at $T = 0$. The key indicates the pressure in bars for each curve, and these pressures correspond to densities of 0.11, 0.12, 0.13, 0.14, and 0.15 g cm^{-3}. The dispersion curves are calculated from the density functional of Dalfovo *et al.* (Ref. 15).

In (5) the coefficients α_i and γ_{ij} are assumed to be independent of density and their values are listed in Ref. 15. The response function χ_q is given by a complicated expression (Eq. (11) of Ref. 15). For a given choice of the density, it is straightforward to calculate the dispersion curve numerically, and results for several densities in the negative pressure range are shown in Fig. 4. It can be seen that as the density is decreased, the sound velocity decreases, the maxon energy decreases and the roton energy increases.

4. INTERACTIONS BETWEEN EXCITATIONS

According to the Landau approach, the density of the normal fluid component at temperature T is given by the formula

$$\rho_n(T) = \frac{\hbar^2}{3kTV} \sum_{\vec{q}} \bar{n}^0_{\vec{q}}(\bar{n}^0_{\vec{q}} + 1)\, q^2, \tag{6}$$

where $\bar{n}^0_{\vec{q}} \equiv [\exp(\varepsilon^0_{\vec{q}}/kT) - 1]$ is the equilibrium number of excitations of momentum $\vec{q}$, and the integral goes over the spectrum of elementary excitations. Using this formula, the lambda temperature can be calculated as the temperature at which the normal fluid density becomes equal to the total density of the liquid.[8] However, it is known that this gives too high a

result for T_λ. For example, at the saturated vapor pressure, the density at T_λ is 0.146 g cm^{-3}. If we use the dispersion curve for this density, we find that ρ_n does not become equal to ρ until a temperature of 2.75 K is reached. The actual lambda temperature is 2.17 K.

To obtain a more accurate estimate of T_λ, it is necessary to allow for the fact that at high temperatures the density of excitations becomes very large and consequently interactions between the excitations are important. The energy ε_q of an excitation then depends on temperature. This shift in the dispersion curve with temperature has been measured in neutron scattering experiments. A number of different approaches have been used to allow for this.[21–25] In this paper, we use a modification of the theory developed by Bedell, Pines, and Fomin (BPF)[24] that they refer to as roton liquid theory. Following the method used in Landau's Fermi liquid theory, the Helmholtz free energy of the liquid is written as an expansion at constant density to second order in the number of rotons

$$F = F_0 + \sum_{\vec{q}} n_{\vec{q}} \varepsilon^0_{\vec{q}} + \frac{1}{2V} \sum_{\vec{q}\vec{q}'} f_{\vec{q}\vec{q}'} n_{\vec{q}} n_{\vec{q}'} - TS, \tag{7}$$

where F_0 is the free energy in the ground state at the same density, and S is the entropy, given by

$$S = k \sum_{\vec{q}} [(1+n_{\vec{q}}) \ln(1+n_{\vec{q}}) - n_{\vec{q}} \ln n_{\vec{q}}]. \tag{8}$$

The function $f_{\vec{q}\vec{q}'}$ describes the interaction between excitations with wave vectors $\vec{q}$ and $\vec{q}'$. The equilibrium distribution of excitations is obtained by minimizing the free energy, and the result is

$$\bar{n}_{\vec{q}} = 1/[\exp(\varepsilon_{\vec{q}}/kT) - 1], \tag{9}$$

where

$$\varepsilon_{\vec{q}} = \varepsilon^0_{\vec{q}} + \frac{1}{V} \sum_{\vec{q}'} f_{\vec{q}\vec{q}'} \bar{n}_{\vec{q}'} \tag{10}$$

is the effective excitation energy at temperature T. For a given form of $f_{\vec{q}\vec{q}'}$, Eqs. (9) and (10) have to be solved self consistently to determine the equilibrium distribution function $\bar{n}_{\vec{q}}$. The free energy and entropy can then be determined from Eqs. (7) and (8).

BPF point out that if the temperature is such that most of the excitations have momenta near to the roton minimum, the function $f_{\vec{q}\vec{q}'}$ can be considered to depend only on the angle $\theta_{\vec{q}\vec{q}'}$ between $\vec{q}$ and $\vec{q}'$. In this case,

$$f_{\vec{q}\vec{q}'} = \sum_l f_l P_l(\cos \theta_{\vec{q}\vec{q}'}). \tag{11}$$

where the f_l depend solely on the density. The effective roton energy gap then varies with temperature as

$$\Delta(T) = \Delta_0 + f_0 \bar{n}_r(T), \tag{12}$$

where $\bar{n}_r(T)$ is the number of rotons per unit volume calculated using the distribution function $\bar{n}_{\vec{q}}$ given by Eq. (9). Equation (12) follows from (10) when the sum is restricted to momenta $\vec{q}'$ in the region of the roton minimum.

For the purposes of the present paper it is convenient to replace Eq. (11) by the expression

$$f_{\vec{q}\vec{q}'} = \frac{\varepsilon^0_{\vec{q}} \varepsilon^0_{\vec{q}'}}{\Delta_0^2} \sum_l f_l P_l(\cos\theta_{\vec{q}\vec{q}'}), \tag{13}$$

where Δ_0 is the roton energy gap at zero temperature, and *not* to restrict the sums over wave vectors to the region of $\vec{q}$-space close to the roton minimum. Clearly, this procedure will give the same result as the BPF theory if the main contributions to the sums do in fact arise from this region of the roton minimum. If the contributions from other regions of momentum space become significant, Eq. (13) assumes that the effect of the interactions on a given excitation is proportional to its energy. We have assumed this so that the interaction becomes appropriately weak for very low energy excitations. A more accurate form for $f_{\vec{q}\vec{q}'}$ could perhaps be found from results such as those in Refs. 25 and 26 but we have preferred to use Eq. (13) for simplicity. As we shall see, our model gives quite good agreement with experiment.

With the use of Eq. (13), Eq. (10) becomes

$$\varepsilon_{\vec{q}} = \varepsilon^0_{\vec{q}} \left(1 + \frac{f_0 X(T)}{\Delta_0^2} \right), \tag{14}$$

where

$$X(T) = \frac{1}{V} \sum_{\vec{q}} \varepsilon^0_{\vec{q}} n_{\vec{q}}. \tag{15}$$

The thermodynamics of the liquid is calculated from a self-consistent solution of Eqs. (9), (14), and (15).

A. Determination of f_0

As noted by BPF, the value of f_0 determines the extent to which the energy of the elementary excitations decreases as the temperature is raised.

This change in energy occurs principally as the temperature approaches the lambda point. For positive pressures, we can select a value of f_0 such that the entropy at T_λ has the value found experimentally. In Fig. 5, we show how the product $n_4 f_0$ determined in this way changes with density in the pressure range from P_{SVP} up to 15 bars using data from Refs. 27 and 28 and summarized in Table I of Ref. 22. It can be seen that over this pressure range the variation of $n_4 f_0$ is only 3%. It would be a reasonable approximation to assume that $n_4 f_0$ is constant over the entire pressure range. However, in the negative pressure regime, we have chosen the linear extrapolation of $n_4 f_0$ shown in Fig. 5, namely

$$n_4 f_0 = (-10.197 + 21.12\rho)\ K, \tag{16}$$

with ρ in g cm^{-3}. If we make a fourth order polynomial of $n_4 f_0$ in the range 0 to 20 bars and then extend this down to -9 bars, the result is -9.2 K, i.e., about 20% more negative than obtained with the linear fit.

The value of $n_4 f_0$ that we have found (around -7 K at positive pressures) is significantly smaller than the result (-9.67 K) obtained by BPF[24] at P_{SVP}. We have investigated the reason for this difference. BPF adjust $n_4 f_0$ so that the calculated specific heat in the temperature range 1.5 to 2.1 K is in good agreement with experiment, whereas we have chosen $n_4 f_0$ so that the entropy at the lambda point has the correct value. Using our model, we find that the value of $n_4 f_0$ is only slightly changed if we fit the specific heat rather than the entropy, and so the reason for the difference

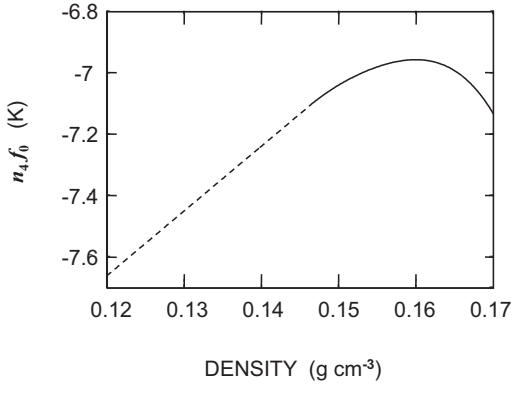

Fig. 5. The roton liquid interaction parameter f_0 multiplied by the number density n_4 as a function of density. The solid curve is the results of a fit to experimental data as explained in the text. The dashed line is the extrapolation into the negative pressure regime using Eq. (16).

TABLE I

Calculated Properties of the Liquid Along the Spinodal Line

Temperature (K)	Density (g cm $^{-3}$)	Entropy (J g $^{-1}$ K $^{-1}$)	Pressure (bars)
0.1	0.1058	0.0013	−9.53
0.2	0.1061	0.0039	−9.52
0.3	0.1065	0.0076	−9.51
0.4	0.1068	0.0122	−9.49
0.5	0.1071	0.0178	−9.46
0.6	0.1073	0.0244	−9.44
0.7	0.1076	0.0322	−9.40
0.8	0.1079	0.0414	−9.36
0.9	0.1082	0.0529	−9.32
1.0	0.1085	0.0680	−9.27
1.1	0.1088	0.0886	−9.21
1.2	0.1091	0.117	−9.14
1.3	0.1094	0.156	−9.06
1.4	0.1098	0.209	−8.97
1.5	0.1101	0.279	−8.87
1.6	0.1105	0.369	−8.75
1.7	0.1110	0.485	−8.61
1.8	0.1114	0.633	8.45
1.9	0.1120	0.826	−8.26
2.0	0.1127	1.08	−8.03
2.1	0.1136	1.45	−7.72
2.15	0.1145	1.72	−7.51
2.17	0.1151	1.87	−7.40
2.18	0.1156	1.96	−7.33

must lie elsewhere. It appears that the important difference in the two calculations comes from the momentum range of the excitations that are considered. BPF include only the roton contribution to the thermodynamic quantities. For non-interacting excitations ($n_4 f_0 = 0$), we find that the calculated entropy at T_λ is $S_\lambda^0 = 0.76$ J g $^{-1}$ K $^{-1}$ when the momentum range is restricted to the roton region (1.5 to 2.3 Å $^{-1}$), whereas S_λ^0 is 0.91 J g $^{-1}$ K $^{-1}$ when the entire range of momentum is included. A smaller value of S_λ^0 means that a larger value of $n_4 f_0$ is required to increase the entropy up to the experimental value. When we repeat our calculation restricting the momentum range to 1.5 to 2.3 Å $^{-1}$, we obtain $n_4 f_0 = -9.4$ K, in reasonable agreement with the result of BPF.

B. Determination of f_1

To calculate the normal fluid density ρ_n, we give the distribution of excitations a small momentum density $\vec{J}$. The free energy $F' = F - \vec{v}.\vec{J}$ is

then minimized at fixed $\vec{J}$; the drift velocity $\vec{\mathrm{v}}$ acts as a Lagrange multiplier. This gives a distribution function that differs from the static distribution $\bar{n}_q$ by a small amount $\delta n_{\vec{q}}$. We write this change as

$$\delta n_{\vec{q}} = -\vec{q}.\vec{\mathrm{v}}(1+\chi_{\vec{q}})\frac{\partial \bar{n}_{\vec{q}}}{\partial \varepsilon_{\vec{q}}} \tag{17}$$

The factor $\chi_{\vec{q}}$ represents the effect of the $f_1 \cos(\theta_{\vec{q}\vec{q}'})$ term on the excitation energy. If $f_1 > 0$, the effect of the interaction is to reduce the polarization of the momentum distribution along the direction of $\vec{\mathrm{v}}$ so that, for $f_1 > 0$, we expect $\chi_{\vec{q}} < 0$. We determine $\chi_{\vec{q}}$ self-consistently. From Eqs. (10) and (11), the contribution to the excitation energy from the f_1 term is

$$-\vec{q}.\vec{\mathrm{v}}\chi_{\vec{q}} = \frac{1}{V}\sum_{\vec{q}'} f_1 \frac{\varepsilon^0_{\vec{q}}\varepsilon^0_{\vec{q}'}}{\Delta_0^2}\cos(\theta_{\vec{q}\vec{q}'})(-\vec{q}'.\vec{\mathrm{v}})(1+\chi_{\vec{q}'})\frac{\partial \bar{n}_{\vec{q}'}}{\partial \varepsilon_{\vec{q}'}} \tag{18}$$

The solution for $\chi_{\vec{q}}$ is

$$\chi_{\vec{q}} = -\frac{X(T)}{3kT}\frac{f_1 \varepsilon^0_{\vec{q}}}{q\Delta_0^2}\frac{Q_{11}}{1+\dfrac{f_1 Q_{20}}{3kT\Delta_0^2}}, \tag{19}$$

where

$$Q_{\alpha\beta} \equiv \frac{1}{V}\sum_{\vec{q}} \bar{n}_{\vec{q}}(1+\bar{n}_{\vec{q}})(\varepsilon^0_{\vec{q}})^{\alpha} q^{\beta}. \tag{20}$$

The normal fluid density is determined by the equation

$$\vec{J} \equiv \rho_n \vec{\mathrm{v}} = \frac{1}{V}\sum_{\vec{q}} \vec{q}\,\delta n_{\vec{q}}. \tag{21}$$

This gives

$$\rho_n = \frac{1}{V}\sum_{\vec{q}} \frac{\hbar^2 q^2}{3kT}\bar{n}_{\vec{q}}(\bar{n}_{\vec{q}}+1)\frac{1+\dfrac{f_1}{3kT\Delta_0^2 Q_{02}}(Q_{02}Q_{20}-Q_{11}^2)}{1+\dfrac{f_1 Q_{20}}{3kT\Delta_0^2}} \tag{22}$$

When $f_1 = 0$, this reduces to an expression of the form of Eq. (6), but with $\bar{n}^0_{\vec{q}}$ replaced by $\bar{n}_{\vec{q}}$. If all the excitations are very near to the region of the roton minimum, we have

$$Q_{02} \approx \bar{n}_r p_0^2, \qquad Q_{20} \approx \bar{n}_r \Delta_0^2, \qquad Q_{11} \approx \bar{n}_r p_0 \Delta_0, \tag{23}$$

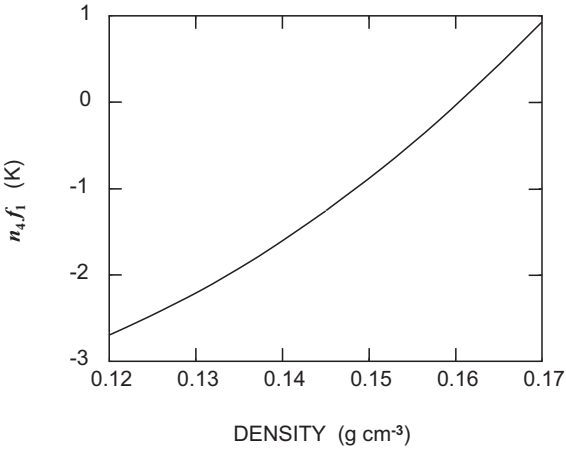

Fig. 6. The roton liquid parameter f_1 multiplied by the number density n_4 as a function of density as given by Eq. (25).

where $\bar{n}_r$ is the average number of rotons per unit volume. In this case, Eq. (22) reduces to the result of BPF:

$$\rho_n = \frac{1}{V}\sum_{\vec{q}} \frac{\hbar^2 q^2}{3kT}\bar{n}_{\vec{q}}(\bar{n}_{\vec{q}}+1)\frac{1}{1+\dfrac{\bar{n}_r f_1}{3kT}}. \tag{24}$$

To estimate f_1, we adjust its value so that the normal fluid density given by Eq. (22) equals the total density at the lambda point. We again use the experimental data in Refs. 27 and 28. The results are shown in Fig. 6. The expression

$$n_4 f_1 = (0.8809 - 101.86\rho + 600.7\rho^2)\ \text{K} \tag{25}$$

gives a very good fit to the values of $n_4 f_1$ throughout the density range 0.145 to 0.17 g cm^{-3}. We will use this same expression for negative pressures.

C. Test of Model

The value of f_0 has been chosen so that for values of the density and temperature corresponding to a point on the lambda line, the entropy has the value determined experimentally. As a test of the model, we have calculated the value of the pressure along the lambda line and the results are

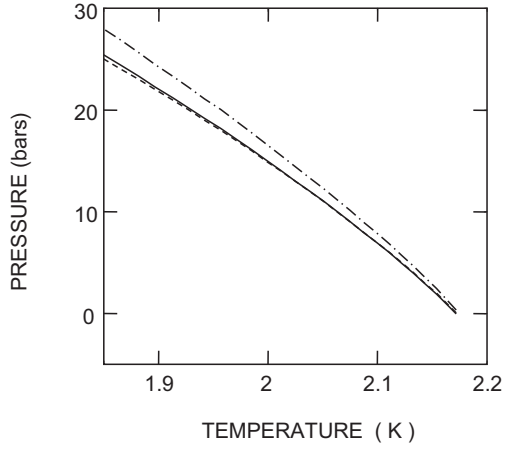

Fig. 7. Location of the lambda line in the P-T-plane. The solid curve is from experiment (Ref. 28). The dashed line is calculated including the interaction between excitations, and the dashed-dotted line is the calculated result when interactions are neglected.

shown in Fig. 7. The pressure was obtained by numerically calculating the free energy at two closely spaced densities in order to find its derivative with respect to density. Rather than using (7) directly, the free energy is most easily found from the entropy, Eq. (8), and the internal energy per unit volume derived from (7)

$$e(\rho, T) = e(\rho, 0) + X(T)[1 + \tfrac{1}{2} f_0 X(T)/\Delta_0^2] \tag{26}$$

Figure 7 shows that the agreement with experiment is very good; the difference between the experimental and calculated pressure varies from 0.1 bars at low pressures to -0.4 bars at P_λ of 25 bars. Also shown in Fig. 7 is the dotted line: the pressure along the lambda line calculated with f_0 set equal to zero. It can be seen that the calculated pressure is then in poor agreement with experiment.

As a second test of the model, we have calculated the specific heat C_V at constant volume at densities of 0.15 and 0.17 g cm^{-3} with the results shown in Fig. 8. The calculation is compared with the data of Lounasmaa.[29] Since f_0 has been adjusted to give the correct entropy at the lambda point, if C_V is too low over one temperature range there must be another range in which it is larger than found experimentally. It can be seen that our model overestimates the specific heat near the lambda point, but underestimates it at lower temperatures. At 1.6 K and $\rho = 0.17$ g cm^{-3}, for example, the calculated specific heat is 10% too small. At this temperature,

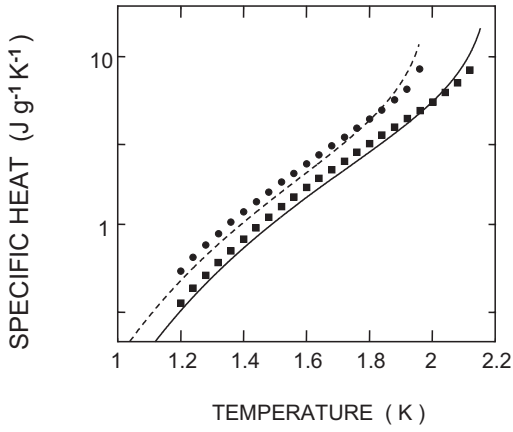

Fig. 8. The specific heat per unit mass calculated for densities of 0.15 (solid curve) and 0.17 g cm^{-3} (dashed curve). The squares and circles are experimental data from Ref. 29.

the effect of interactions between excitations is still small, and so the discrepancy must arise from an incorrect excitation dispersion curve. The discrepancy would be removed if the roton energy gap at this density were taken to be about 2% smaller. This is the difference between the roton gap calculated from the density functional of Dalfovo *et al.*, and the gap measured experimentally. It is clear that if the roton gap were reduced so as to increase the specific heat in the low temperature range, a smaller magnitude of f_0 would be needed to give S_λ the correct value. This would then improve the agreement between the model and the experimental values of C_V near to T_λ. Possibly the density functional of Dalfovo et al could be refit to give better agreement with experiment. However, we felt that this was beyond our capabilities and outside the scope of the present paper.

5. THERMODYNAMICS IN THE NEGATIVE PRESSURE REGIME

In this section we present the results of calculations of the thermodynamic functions based on the formulas derived so far.

A. Location of the Spinodal Line

To determine the spinodal pressure for a temperature T, we calculate the pressure as the density is decreased, and find the density at which the pressure becomes a minimum. The results are listed in Table I and shown

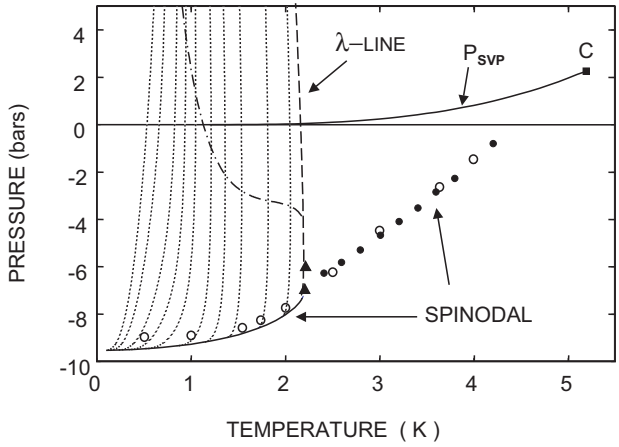

Fig. 9. The calculated phase diagram of helium. The lambda line (dashed curve) and spinodal (solid curve) for the superfluid phase are calculated as described in the text. The dotted curves are lines of constant entropy for entropies of 0.001, 0.002, 0.005, 0.01, 0.02, 0.05 0.1, 0.2 0.5, 1.0, and 2 J g^{-1} K^{-1}. The dot-dash curve is a line of minimum density where the thermal expansion coefficient is zero. The spinodal for the normal liquid (solid circles) is from the estimate made in Ref. 7. The spinodal from the path-integral Monte Carlo calculation by Bauer *et al.* (Ref. 9) is indicated by the open circles, and the solid triangles are their results for the lambda line. The curve showing the saturated vapor pressure P_{SVP} and the location of the critical point are the standard experimental values.

in Fig. 9. We have included in this figure the estimate of the spinodal location for the normal liquid made by Hall and Maris,[7] and the path-integral Monte Carlo results of Bauer *et al.*[9] for the superfluid phase.

B. Location of the Lambda Line

To determine the location of the lambda line, we calculate the normal fluid density as a function of density and temperature using Eq. (22), and for each density find the temperature T_λ at which ρ_n becomes equal to ρ. The results are shown in Table II, and plotted in Fig. 9. Although this is difficult to see in the graph, as the pressure decreases towards more negative values, T_λ increases but then decreases as the spinodal is approached. This decrease is due to the increase in the contribution to ρ_n from the phonons as the pressure is lowered, and also to the decrease in the density ρ itself which has the result that the normal fluid density becomes equal to the total density at a lower temperature. The maximum value of T_λ is 2.205 K at a pressure $P_\lambda^{\max}$ of about -5.7 bars, and the lambda line meets

TABLE II

Calculated Properties of the Liquid Along the Lambda Line

Pressure (bars)	Temperature (K)	Density (g cm $^{-3}$)	Entropy (J g $^{-1}$ K $^{-1}$)
−0	2.172	0.1463	1.560
−1	2.180	0.1442	1.586
−2	2.188	0.1419	1.614
−3	2.195	0.1393	1.647
−4	2.200	0.1363	1.683
−5	2.204	0.1328	1.731
−6	2.205	0.1283	1.794
−7	2.197	0.1211	1.903

the spinodal at a pressure of −7.3 bars and a temperature of 2.18 K. Bauer *et al.* have performed path-integral Monte Carlo calculations of T_λ for two densities.[9] Their results are included in Fig. 9 and they are in very good agreement with our findings.

C. Entropy for Negative Pressures

In experiments to study cavitation, liquid at an initial pressure at or above the saturated vapor pressure is expanded until bubbles nucleate. During this expansion, both the pressure and the temperature change. If the coupling to second sound is neglected,[30] the state of the liquid moves along a line of constant entropy in the P-T plane. We have determined the

TABLE III

Calculated Pressure and Temperature of Liquid at Selected Values of the Entropy. The Entropy S Is in Units of J g $^{-1}$ K $^{-1}$. The Last Row of the Table Gives the Entropy at the Spinodal Pressure P_c

Pressure (bars)	T ($S = 0.001$) (K)	T ($S = 0.01$) (K)	T ($S = 0.1$) (K)	T ($S = 1$) (K)
0	0.532	0.937	1.360	2.047
−1	0.513	0.932	1.362	2.051
−2	0.493	0.924	1.362	2.053
−3	0.471	0.913	1.362	2.055
−4	0.446	0.899	1.360	2.055
−5	0.420	0.877	1.355	2.052
−6	0.389	0.845	1.346	2.046
−7	0.352	0.797	1.331	2.032
−8	0.307	0.720	1.302	1.990
−9	0.232	0.581	1.216	–
P_c	0.102	0.327	1.072	1.918

location of these lines for selected values of the entropy and they are included in Fig. 9 and in Table III. We have also calculated the entropy on the lambda line, shown in Table II.

On a line in the P-T plane where $(\partial S/\partial P)_T$ vanishes, the thermal expansion coefficient α is zero. This line on which $\alpha = 0$ (the line of minimum density) is included in Fig. 9. At temperatures and pressures below this line, the expansion coefficient is positive because of the enhanced contribution to the entropy from the phonons at lower temperatures and pressures. Above the line, the rotons are more important.

It can be seen from Fig. 9 that, according to the Landau theory, the line on which $\alpha = 0$ intersects the lambda line at around -4 bars at a finite angle. This conclusion is corrected in Appendix B, where we take into account the known critical properties of helium near the lambda line. According to Appendix B, the $\alpha = 0$ line meets the lambda line tangentially at a pressure $P_\lambda(\alpha = 0)$ that is estimated to be about -5.3 bars.

Although it is not shown in Fig. 9, there is another line of zero α just above the lambda line; in this case a line of maximum density. As described in Appendix B, this He I line also meets the lambda line tangentially at $P_\lambda(\alpha = 0)$.

In Fig. 10 we show the specific heat at constant volume for densities from 0.12 to 0.15 g cm^{-3}. At low temperatures the specific heat is dominated by the contribution from phonons and varies as T^3. As the pressure becomes more negative, the phonon specific heat becomes larger, and it continues to be the dominant contribution to the specific heat up to

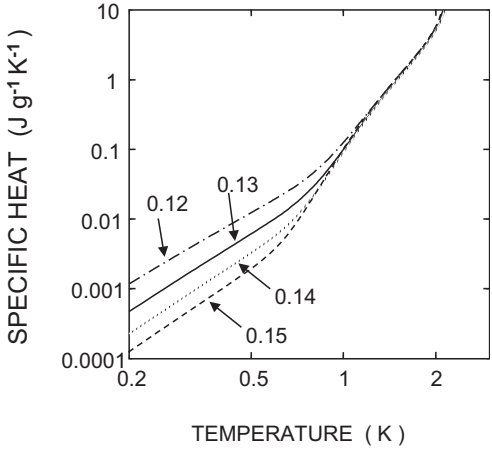

Fig. 10. Calculated specific heat at constant volume as a function of temperature for densities of 0.12, 0.13, 0.14, and 0.15 g cm^{-3}.

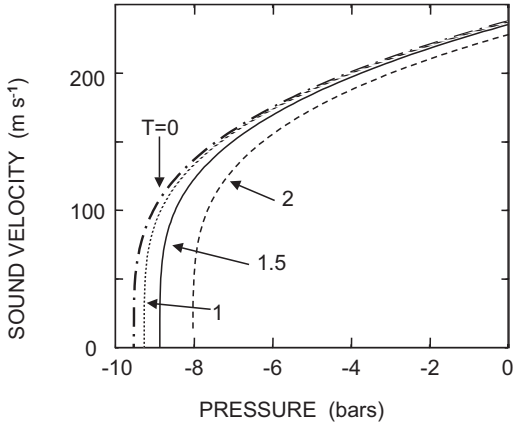

Fig. 11. Calculated first sound velocity as a function of pressure at temperatures of 0, 1, 1.5, and 2 K.

higher temperatures. Above about 1 K, on the logarithmic scale of the graph, the specific heat is nearly independent of density.

D. First and Second Sound Velocities

From the second derivative of the free energy with respect to density, we have calculated the isothermal bulk modulus. In Fig. 11, we show the variation of the isothermal sound with pressure at various temperatures. It

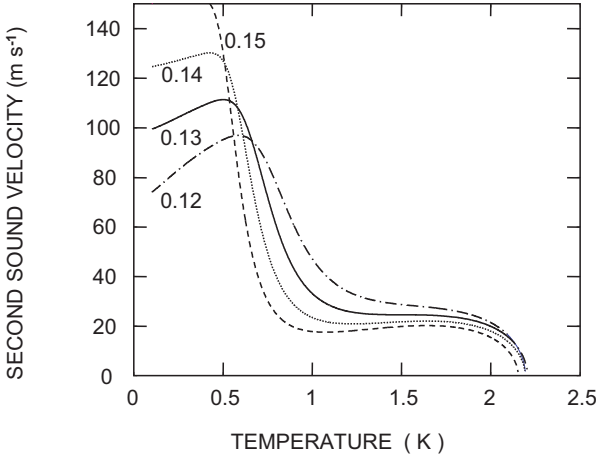

Fig. 12. Calculated second sound velocity at constant volume as a function of temperature for densities of 0.12, 0.13, 0.14, and 0.15 g cm^{-3}. The temperature dependence in the phonon region is due to the strong phonon dispersion at low densities (see Fig. 4).

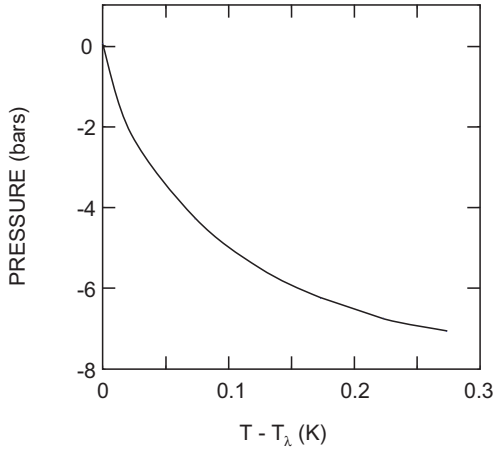

Fig. 13. Calculation of the result of an isentropic expansion starting from states on the saturated vapor pressure line in liquid helium I. The graph shows the negative pressure reached on the lambda line starting at a temperature interval above the lambda point.

can be seen that c changes little between $T = 0$ K and 1 K. The second sound velocity calculated from the entropy, normal fluid density, and the specific heat is shown in Fig. 12. In the low temperature region, where c_2 approaches the limit $c/\sqrt{3}$, there is a marked temperature dependence at negative pressures. This is due to the strong phonon dispersion at low densities, shown in Fig. 4.

E. Isentropic Expansion from Helium I

In cavitation experiments, the expansion of the liquid may be approximated as isentropic. Figure 13 shows our calculation of the pressure on the lambda line reached by isentropic expansion from various states on the saturated vapor pressure line in helium I. The entropy in He I was taken from Lounasmaa.[29] Because of uncertainties in the temperature scale, we have plotted the graph in terms of the initial temperature interval $T - T_\lambda$ above the lambda point.

F. Difficulties Near the Spinodal

As explained in Sec. IV, the calculations described here take account of the interactions between excitations in an approximate way by using roton liquid theory. This method is primarily directed to allowing for the

interactions of high-energy excitation that make the major contribution to the thermodynamics as the lambda temperature is approached. Although we have modified the original roton liquid formulas to include interactions at all energies, for simplicity we have not attempted to do this in an accurate way. However, it is important to note that the theory we have described is not internally consistent as the spinodal is approached. To calculate thermodynamic quantities, we have used the $T = 0$ dispersion curve from the density-functional theory of Dalfovo *et al.*,[15] and applied a correction to the quasi-particle energy given by Eq. (14). Even with this correction, when the temperature is non-zero the velocity of very low energy phonons does not vanish as the spinodal pressure $P_c(T)$ is approached. Rather, the phonon velocity goes to zero only when the pressure reaches $P_c(T = 0)$. To help to correct this problem, we ought to use an accurate formula for $f_{\vec{q}\vec{q}'}$ as $q \to 0$. Fortunately, it appears that the inconsistency leads to only a small error in the final results. At low temperatures, below 0.6 K, the spinodal pressure deviates only slightly from its low temperature limiting value. At high temperatures, the shift in the spinodal becomes large, but then the low energy phonons make only a small contribution to the thermodynamics and so an error in their treatment leads to only a small error in the final result.

6. SUMMARY

We have calculated the thermodynamic functions of superfluid helium in the metastable negative pressure regime. We have used the Landau approach in which all thermodynamic quantities are expressed as sums over the distribution of elementary excitations. Interactions between elementary excitations are important near the lambda line and are allowed for in an approximate way through the introduction of two roton liquid parameters. For positive pressures, these parameters f_0 and f_1 are determined by comparison of the calculated normal fluid density and entropy at the lambda line with experimentally measured values. In the negative pressure regime, f_0 and f_1 are estimated by extrapolation from positive pressures. The results obtained depend on the assumption that these extrapolations are reasonable. The results of our calculations should be helpful in the analysis of cavitation experiments and other measurements in superfluid helium at negative pressures.

APPENDIX A: EQUATION OF STATE AT $T = 0$ K

The original calculation of the equation of state contained a small error coming from confusion over bars and atmospheres. We thank

F. Caupin and S. Balibar for pointing this out. With this correction the value of the density ρ_c at the spinodal becomes 0.094262 g cm^{-3}, the constant $b = 1.4054 \times 10^6$ g^{-1} cm^4 s^{-1} in Eq. (1), and $P_c = -9.6201$ bars. The relation between the pressure and the density is given by the formula

$$P = P_c + \frac{b^2}{27}(\rho - \rho_c)^3 \tag{A1}$$

and the energy per unit volume is

$$e(\rho) = \frac{b^2}{9}\left(\frac{\rho^3}{6} - \rho_c\rho^2 + \rho_c^2\rho \log_e(\rho/\rho_0) + s\rho + \frac{\rho_c^3}{3} - \frac{9P_c}{b^2}\right) \tag{A2}$$

where

$$s = \frac{1}{\rho_0}\left(\frac{9e_0}{b^2} - \frac{\rho_0^3}{6} + \rho_0^2\rho_c - \frac{\rho_c^3}{3} + \frac{9P_c}{b^2}\right). \tag{A3}$$

with e_0 and ρ_0 the density and energy per unit volume, respectively, at zero pressure. For ρ_0 we use the value 0.14513 g cm^{-3} from Ref. 31 and $e_0 = -2.162 \times 10^7$ erg cm^{-3} from Ref. 32.

APPENDIX B: EXPANSION COEFFICIENT AT THE LAMBDA LINE

Skripov[10] has raised some interesting questions about the expansion coefficient α in helium at negative pressures. At both positive and negative pressures, α is positive at low T because the phonon entropy decreases as the pressure increases. At higher temperatures, the rotons become more important and α changes sign on the dot-dashed $\alpha = 0$ line shown in Fig. 9. There is another $\alpha = 0$ line in the He I region (not shown in the figure) a few millikelvin above the lambda line. The Landau theory we have used in the main part of this paper does not apply in He I, nor does it predict the correct critical behavior at the lambda transition. (However, as we have seen, it gives quite accurate values of the entropy and normal density at the lambda line.) In this Appendix, we discuss the intersection of the two $\alpha = 0$ lines with the lambda line in terms of the known critical properties of helium.

Neglecting finite-size effects and higher order terms in t, the heat capacity in the neighborhood of the lambda line is[33, 34]

$$\begin{aligned} C_p(P,T) &= C_\lambda(P) - A(P)\,t^\beta \qquad T > T_\lambda \\ C_p(P,T) &= C_\lambda(P) - A'(P)\,t^\beta \qquad T < T_\lambda \end{aligned} \tag{B1}$$

where

$$t \equiv |T - T_\lambda(P)|, \tag{B2}$$

and the exponent β is universal and, in our notation, equal to $\sim +0.013$, independent of pressure. We note that A and A' are positive, and there is no discontinuity[35] in the specific heat at the lambda line, where it has the value $C_\lambda(P)$.

From (B1) and (B2), the entropy for small t is approximately

$$\begin{aligned} S &\approx S_\lambda(P) - At^{\beta+1}/[T_\lambda(\beta+1)] + C_\lambda t/T_\lambda; \qquad T > T_\lambda \\ S &\approx S_\lambda(P) + A't^{\beta+1}/[T_\lambda(\beta+1)] - C_\lambda t/T_\lambda; \qquad T < T_\lambda \end{aligned} \tag{B3}$$

Using the Maxwell relation $(\partial V/\partial T)_P = -(\partial S/\partial P)_T$ and retaining only the lowest terms in t, Eq. (B3) predicts that the isothermal expansion coefficient above and below the lambda line is

$$\alpha = \frac{1}{V_\lambda}\left[\frac{C_P(t)}{T_\lambda}\frac{dT_\lambda}{dP} - \frac{dS_\lambda}{dP}\right] \tag{B4}$$

where V_λ is the volume at the lambda line. Equation (B4) shows that the expansion coefficient has the same kind of singular behavior as the specific heat. However, at pressures above $P_\lambda^{\max} \sim -5.7$ bar, where T_λ has its maximum value, the value of dT_λ/dP is negative so that α has a downward cusp at the lambda line. At pressures below $P_\lambda^{\max}$ there is an upward cusp in α as there is in the specific heat.

From Eq. (B4), the value of α at the lambda line ($t = 0$) is

$$\alpha_\lambda = \frac{1}{V_\lambda}\left[\frac{C_\lambda}{T_\lambda}\frac{dT_\lambda}{dP} - \frac{dS_\lambda}{dP}\right] \tag{B5}$$

This is negative at higher pressures until, at a pressure $P_\lambda(\alpha = 0)$ just above the maximum in T_λ, it changes sign. (Note that, according to Table II, the quantity dS_λ/dP is always negative.) According to our extrapolation of the line $\alpha = 0$ in the He II region the pressure $P_\lambda(\alpha = 0)$ is approximately -4 bar.

A better estimate of $P_\lambda(\alpha = 0)$ can be made using Eq. (B5). Assuming that the value of C_λ at negative pressures is about 10^2 J g^{-1} K^{-1} as it is at zero pressure, we find that $P_\lambda(\alpha = 0) \approx -5.3$ bars, i.e., about 0.4 bar above the pressure $P_{\lambda\max}$, the pressure at the maximum in T_λ. This estimate, $P_\lambda(\alpha = 0)$ bar, was made by fitting T_λ and S_λ to polynomials in P and then differentiating to obtain dS_λ/dP and dT_λ/dP.

Since there is no jump in α at the superfluid transition, the line $\alpha = 0$ on the high temperature He I side must also intersect the lambda line at the pressure $P_\lambda(\alpha = 0)$. Although the two $\alpha = 0$ lines intersect the lambda line at the same point, the He II line is a line of minimum density, while the He I line is a line of maximum density.

An inspection of Eq. (B4) at small t shows that, near to $P_\lambda(\alpha = 0)$, the $\alpha = 0$ lines in He I and He II approach each other and the lambda line according to the formula

$$t^\beta \propto P - P_\lambda(\alpha = 0) \tag{B6}$$

Therefore they osculate the lambda line, approaching it at zero angles.

ACKNOWLEDGMENTS

We thank S. Balibar, F. Caupin, F. Gasparini, and S. Mukherjee for helpful discussions. This work was supported in part by the National Science Foundation through grant DMR-0071507. One of the authors, Edwards, would like to thank Brown University Physics Department for its hospitality during November 2001 when some of this work was performed.

REFERENCES

1. For a review, see H. J. Maris, in Proceedings of the 21st International Conference on Low Temperature Physics, Prague, August 1996, *Czech. J. Phys.* **S6**, 2943 (1996).
2. H. J. Maris and S. Balibar, *Physics Today* **53**, 29 (2000).
3. For brevity, we will often refer to the pressure range below the pressure $P_{\rm SVP}$ at which the liquid and vapor are in thermodynamic equilibrium as the negative pressure regime, rather than the regime in which the pressure is less than $P_{\rm SVP}$.
4. S. Balibar, C. Guthmann, H. Lambare, P. Roche, E. Rolley, and H. J. Maris, *J. Low Temp. Phys.* **101**, 271 (1995).
5. S. Balibar, F. Caupin, P. Roche, and H. J. Maris, *J. Low Temp. Phys.* **113**, 459 (1998).
6. S. Balibar and X. Chavanne, unpublished.
7. S. C. Hall and H. J. Maris, *J. Low Temp. Phys.* **107**, 263 (1997).
8. L. D. Landau, *J. Phys. Moscow* **5**, 71 (1941).
9. G. H. Bauer, D. M. Ceperley, and N. Goldenfeld, *Phys. Rev.* **61**, 9055 (2000).
10. V. P. Skripov, *Zh. Fiz. Khim.* **68**, 1382 (1994) [*Russ. J. Phys. Chem.* **68**, 1252 (1994); *Usp. Fiz. Nauk* **170**, 559 (2000); *Phys.-Uspekhi* **43**, 515 (2000)].
11. B. M. Abraham, Y. Eckstein, J. B. Ketterson, M. Kuchnir, and P. R. Roach, *Phys. Rev.* **A1**, 250 (1970).
12. H. J. Maris, *Phys. Rev.* **A5**, 2629 (1973).
13. Q. Xiong and H. J. Maris, *J. Low Temp. Phys.* **77**, 347 (1989).
14. H. J. Maris, *J. Low Temp. Phys.* **94**, 111 (1994).
15. F. Dalfovo, A. Lastri, L. Pricaupenko, S. Stringari, and J. Treiner, *Phys. Rev.* **B52**, 1193 (1995). The equation of state is given in Eq. (13) of this reference. Using the density functional scheme as described there, we have been unable to obtain perfect agreement with the dispersion curve and static response function that they show in their Figs. 1 and 12. For example, we calculate a roton gap that is about 1% higher than shown in their Fig. 12.

16. It appears that the value used by Dalfovo *et al.* (Ref. 12) for the energy per particle was -7.15 K, rather than the value -7.17 K recommended by Ouboter and Yang in Ref. 27. Also the model of Dalfovo *et al.* gives a sound velocity at zero pressure of 2.377×10^4 cm s^{-1}, compared to the value 2.383×10^4 cm s^{-1} measured by Abraham *et al.* in Ref. 11.
17. The way in which the sound velocity goes to zero as the spinodal is approached is an open question. For alternative viewpoints, see M. A. Solis and J. Navarro, *Phys. Rev.* **45**, 13080 (1992) and C. E. Campbell, R. Folk, and E. Krotscheck, *J. Low Temp. Phys.* **105**, 13 (1996). Different assumptions about the way the sound velocity varies as one approached the spinodal pressure lead to slightly different values of P_c.
18. J. Boronat, J. Casulleras, and J. Navarro, *Phys. Rev.* **B50**, 3427 (1994).
19. See, for example, H. R. Glyde, *Excitations in Liquid and Solid Helium*, Oxford University Press, Oxford (1994).
20. A path-integral Monte Carlo calculation of the excitation energy for the single density 0.114 g cm^{-3} and a temperature of 1 K was performed by Bauer *et al.* (Ref. 9). They found the energy at the roton minimum to be approximately 1 K lower than in the Dalfovo *et al.* model. Their result for the maxon energy was also lower. A diffusion Monte-Carlo calculation by J. Boronat and J. Casulleras (*J. Low Temp. Phys.* **110**, 443 (1998)) for a density of 0.113 g cm^{-3} is also in reasonable agreement with the results shown in Fig. 4. At the minimum, their roton energy is about 2 K above that shown in Fig. 4. The statistical error is about 1 K.
21. P. J. Bendt, R. D. Cowan, and J. L. Yarnell, *Phys. Rev.* **113**, 1386 (1959).
22. J. Maynard, *Phys. Rev.* **B14**, 3868 (1976).
23. R. J. Donnelly and P. H. Roberts, *J. Low Temp. Phys.* **27**, 687 (1977).
24. K. Bedell, D. Pines, and I. Fomin, *J. Low. Temp. Phys.* **48**, 417 (1982).
25. K. Bedell, D. Pines, and A. Zawadowski, *Phys. Rev. B* **29**, 102 (1984).
26. K. Fukushima and F. Iseki, *Phys. Rev. B* **38**, 4448 (1988).
27. G. Ahlers, *Phys. Rev.* **A8**, 530 (1973).
28. H. A. Kierstead, *Phys. Rev.* **126**, 153 (1967).
29. O. V. Lounasmaa, *Cryogenics* **1**, 1 (1961).
30. See J. Wilks, *The Properties of Liquid and Solid Helium*, Oxford, London (1967).
31. J. S. Brooks and R. J. Donnelly, *J. Phys. Chem. Ref. Data* **6**, 51 (1977).
32. R. De Bruyn Ouboter and C. N. Yang, in *Physica* **B44**, 127 (1987).
33. See J. A. Lipa, D. R. Swanson, J. A. Nissen, T. C. P. Chui, and U. E. Israelsson, *Phys. Rev. Lett.* **76**, 944 (1996) and the references therein.
34. M. Campostrini, A. Pelissetto, P. Rossi, and E. Vicari, *Phys. Rev. B* **61**, 5905 (2000).
35. We are grateful to Prof. Frank Gasparini for pointing this out.